Bulletin of Environment, Pharmacology and Life Sciences
Bull. Env. Pharmacol. Life Sci., Vol 2 (10) September 2013: 67-78

Online ISSN 2277-1808
Journal's URL:http://www.bepls.com

ORIGINAL ARTICLE

Geometrical Analysis of the Doruneh Anticline (South Kashmar, NE Iran) by Experimental Modeling

Mohammad Mahdi Khatib[1], Tahereh Ghasemi[2] and Mehrvash Nabiei[3]
[1]Assistant professor of Geology, University of Sistan and Balochestan, Zahedan, Iran
[1]Ph.D. student of Geology, University of Sistan and Balochestan, Zahedan, Iran
[1]Ms.c graduated of Geology, University of Sistan and Balochestan, Zahedan, Iran
Email: Elham.nabiei@yahoo.com

ABSTRACT
We study a region of active folding south of the town of Kashmar in NE Iran at 58°-20′ to 59°-10′ west longitude and 34°-56′ to 35°-15′ north latitude. The axial traces of these folds are similar to the trend of adjacent parts of the Doruneh left-lateral fault system. The folds are segmented, with a NW-SE trend in the east, a NE-SW trend in the west, and an east-west trend in the central segment. The folding is related to movements on underlying reverse faults. The folds are asymmetrical with geometry of 1B class. The wavelength of the folds decreases from west to east while the fold amplitude increases. We simulate the Kashmar fold development using a sandbox analogue model with a viscous-plastic decollement within a stratigraphy of alternating layers of gypsum, sand and stone powder. The factors that control the fold shape were studied in four experiments, with variations in decollement surface viscosity and thickness, sedimentary cover height, sedimentary cover layer thicknesses, the total cover sequence and thickness layer of cover sequence. Analysis of our experimental results shows that the Kashmar fold geometry is reproduced when the layer thickness is about one-fifth of the total thickness of the sedimentary cover and the decollemant surface viscosity coefficient is low (in experiment F-2).
Key words: Thrust-related folding, Modelling, Doruneh fault, Kashmar

Received 20.07.2013 Accepted 29.09.2013

INTRODUCTION

In many cases, active thrust faults do not reach Earth's surface, and their existence is instead manifest as uplift and folding. Slip on hidden (blind) faults is associated with the formation of anticlines in the top few kilometers of the Earth's crust [1]. The folding may be associated with the development of secondary normal faults accommodating extension in the outer arc of the fold [2] and slip between bedding layers [3]. Well-exposed fault-related folding is common across Iran and studies in Iran have the potential to show how folds form and develop in general.

The studied area is located to the south of Kashmar at 58°-20′ to 58°-27′ west longitude and 34°-56′ to 35°-15′ north latitude. The anticline hills contain conglomerate rock units with igneous fragments, together with marl and sandstones, which are thought to be of Neogene to Quaternary age. The folds are spread over an east-west length of 63km and a north-south width of 30km. They trend northeast-southwest in the western part, east-west in the central part, and northwest-southeast in the eastern part. The axes of the Kashmar folds are parallel to adjacent parts of the Doruneh left-lateral strike-slip fault, situated ~10 km to the north, which also bends round from a NW-SE trend in the east to a NE-SW trend in the west (Fig. 1).

The origin of Kashmar folds, and their structural relationship to the Doruneh strike-slip fault, has not resolved. It is not known whether the folds have been created due to movement on hidden faults and, if the folds are fault-related, whether they highlight a southwards migration of activity from the Doruneh fault. To solve these issues, we performed detailed analysis of aerial photographs and satellite images of the region, along with the collection of field observations and measurements, in order to characterize the fold geometry. We then attempted to reproduce the observed fold geometries in the laboratory using analogue modeling.

To model the anticline, we first carried out several experiments to study the controlling factors on sediment deformation caused by pressure acting parallel to layering. It is much more difficult to specify the controlling factors when there is a temporal and spatial relationship between faulting and folding. In

these cases, the relationship between faulting and folding could have one of these three possible features: decollement folding [4], thrust-related folding [5, 6], and fault-bend folding [7]. In these models, the faulting occurs either simultaneous with, or prior to, formation of the folds [8].

For example detailed examination of imbricated sheets on the thrust sheets in Norway, suggested an evolutionary model for thrust-related folding [9], and or fault displacements study in the coal basin of South Wariskin in Wales at various scales from micro faults to area scale, suggested that the thrust is created on the decollement surface and in the middle part of the sediment cover, and as the deformation progresses upward and downward, the sedimentary sequence extends [10]. By studying kink bands of North Cody [11] found a connection between kink bands and the faults. By studying the transformation of fault-free kink bands to faulted kink bands he also reached to the conclusion that the position and the direction of faults are controlled by the position and the direction of kink bands.

It is clear from the above examples that, in experimental models and the real world, all thrust-related folds are not formed in the same way. Instead, their deformation mechanism is shifted from shortening parallel to the layering, to the formation of fault-step fragment in the folded layer, and then formation of the thrust-related folding, and at last to fault-bend folding [12].

MATERIALS AND METHODS

Site study

To modeling experiments were performed within a box with 100cm×20cm×20cm dimensions into which another glassy box was put. Quartz sand, plaster, and rock powder were employed to simulate the brittle deformation of sedimentary rocks in thrust wedges. A force, parallel to the layering, was applied by the lever on the sedimentary sequence. The controlling factors of the fold shape were studied in four experiments. In either F-1 and F-4, or F-3 and F-2 experiments, the thickness variation of the layers and the overall thickness of the sedimentary cover over the decollement were investigated, while in the F-1 and F-2 experiments, the decollement surface viscosity and the decollement surface thickness were evaluated.

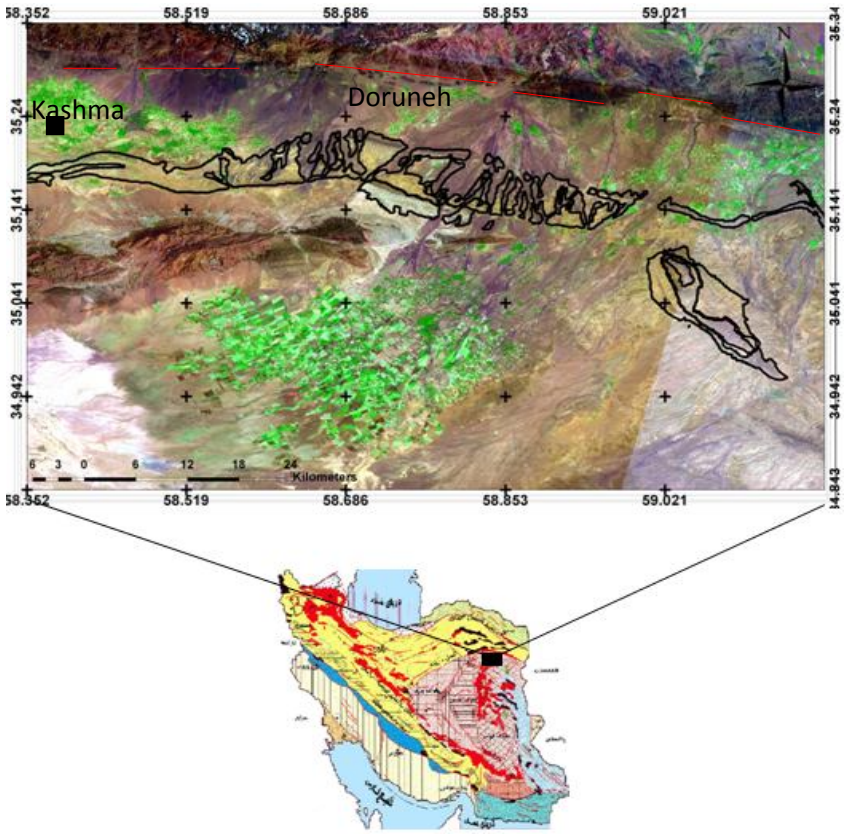

Fig.1.Landsat TM image of the study area. The Kashmar folds trend roughly east-west in the central part of the image. Regions of Neogene outcrop within the fold are outlines in black. The folds are parallel to the Doruneh left-lateral strike-slip fault ~10 km to the north.

The decollement surface is composed of a homogenous mixture of motor oil and plaster with the mixing ratio varying in different experiments. The specific gravities of the materials are as follows: Sand 2.67 gr/mlit, plaster 2.3 gr/mlit, rock powder 2.64 gr/mlit, high viscous decollement surface 1.98 gr/mlit, and low-viscous decollement surface 2.04 gr/milt. The motor oil and the plaster are mixed in the high-viscous decollement layer with a ratio of 2:1, and in the low-viscous decollement layer their mixing ratio is 3:1.
The scaling is selected to be $1/10^5$, which means every 1cm length in the model equates to 1km on the earth. The moving sheet has a constant velocity of 6mm/min. The sequence of layers above the decollement is deformed by under thrusting, which resulted in the formation in all experiments of a coulomb-cone thrust-wedge and thrust-related anticlines.

Analysis of the experiments

In all experiments a coulomb-cone thrust-wedge, together with thrust-related anticlines, develops in a piggy-back sequence with younger structures developing in the foreland of older structures. In experiments F-1 and F-2, three thrust-related folds were formed after cone thrust-wedge. Two of these anticlines were formed close to the moving wall, and the third anticline was created in foreland of the second anticline. Detailed discussion of the thrust-related folds created in four experiments will be presented here.

RESULTS

Experiment

Fig. 2a represents the layers in their initial state. The thickness of each sedimentary cover layer in this experiment is constant and equal to 6mm. The total thickness is 54mm. The decollement surface thickness is small (6mm) and its viscosity is high so that the gravity force on it is equal to:
$W=223157.408\ gr.cm.s^{-2}$
With 2cm shortening, the first thrust and back-thrust was formed (Fig. 2b). With further shortening to 7cm, this thrust was extended and a box fold was created. The second thrust and thrust-tip-related fold was also created at this stage of the experiment (Fig. 2c). With 12cm shortening, the nucleation of the third thrust began, and due to the change in the geometry of the second thrust to flat-ramp-flat, the folding shifted in geometry from a thrust-tip-related fold to a thrust-step-related fold (Fig. 2d).
As deformation progressed more (19cm shortening) the third thrust-step-related anticline was formed whilst the second thrust-step-related fold became narrower (Fig. 2e). With further deformation (24cm shortening) the fourth thrust was created in the third thrust-step-related anticline foreland and over the entire sedimentary cover (Fig. 2f). The box fold was created from the fourth thrust at 29cm shortening (Fig. 2g). The wavelength and the amplitude of these three anticlines in every stage of the measurement experiment are shown in table 1.

Table 1. Measurement of wavelength and amplitude anticlines

Shortening (cm)	Anticline 1		Anticline 2		Anticline 3	
	Wavelength (cm)	Amplitude (cm)	Wavelength (cm)	Amplitude (cm)	Wavelength (cm)	Amplitude (cm)
2	15.2	5.4				
7	12	7				
12	11	7.5				
19	9.4	8.6	6	7.1		
24	8	9.5	6.2	8.4	28.3	6.4
29	4.6	10.6	5.8	10	22.1	8.2

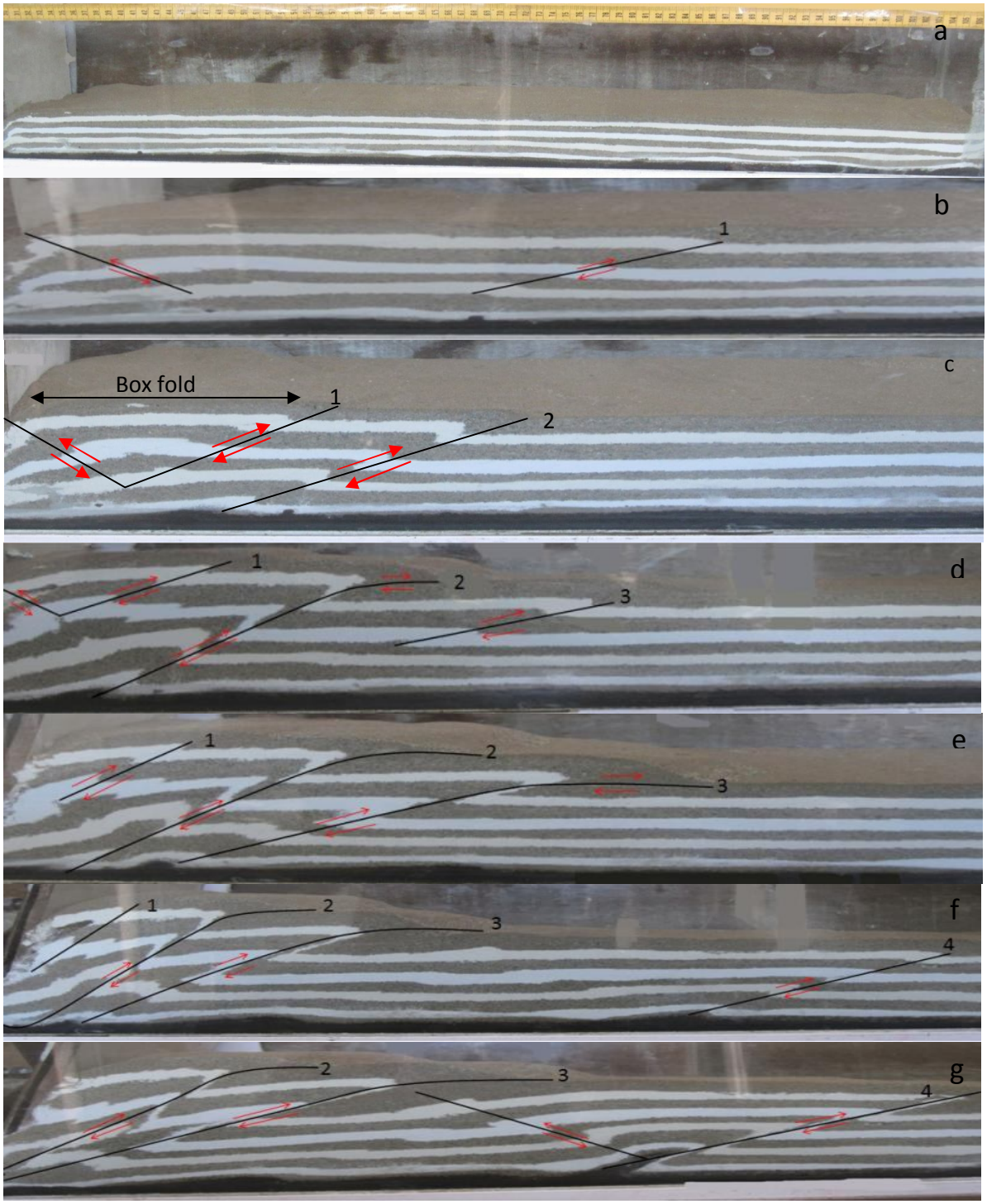

Fig. 2. Different stages of experiment F-1: a) The layered sedimentary sequence at the beginning of the experiment, b) 7cm shortening and appearance of the first thrust and back thrust, c) 12cm shortening and formation of a box fold and the second thrust, d) formation of the anticline relevant to the step of the second thrust and the nucleation of the third thrust, e) 19cm shortening and formation of the anticline relevant to the step of the third thrust, f) appearance of the fourth thrust at 24cm shortening and the fold relevant to the tip of the fourth thrust, g) formation of the box fold at 29cm shortening.

Experiment F-2

The thickness of each layer in this experiment is equal to 12mm; therefore, the total thickness of the sedimentary cover is 60mm (Fig. 2a). The decollement surface is thick (20mm), and its viscosity is low. The gravity force exerted on the decollement surface is equal to:

$$W=2415504.4 \text{ gr.cm.s}^{-2}$$

With 8cm shortening, the first thrust and back-thrust appears in the sedimentary cover (Fig. 2b). In Fig. 2c the anticline related to this thrust is shown. As the deformation continued, a thrust and back thrust

were created in the first anticline foreland (Fig. 2d). In Fig. 2e the formation of the anticline related to this thrust is shown. As the experiment continued, a thrust was created in the second anticline foreland (Fig. 2f). Anticline folding related to this third thrust appears at 30cm shortening. The wavelength and the amplitude of these three anticlines are shown in table 2

Table2. Measurement of wavelength and amplitude anticlines

Shortening (cm)	Anticline 1		Anticline 2		Anticline 3	
	Wavelength (cm)	Amplitude (cm)	Wavelength (cm)	Amplitude (cm)	Wavelength (cm)	Amplitude (cm)
8	12	8.5				
15	14.4	11.2				
18	13.8	11.5	13.5	9		
21	15	13	14.2	10		
25	14.2	12.6	13.4	10.3		
30	13.2	12.8	14.2	11.2	7	27.5

Fig. 3 Different stages of experiment F-2: a) sedimentary layers sequence at the beginning of the experiment, b) formation of the first thrust at 8cm shortening, c) formation of the anticline relevant to thrust first at 15cm shortening, d) formation second thrust in foreland anticline relevant to first thrust in

18cm shortening, e) 21cm shortening and formation of the anticline relevant to second thrust, f) formation third thrust in foreland anticline relevant to second thrust in 25cm shortening.

Experiment F-3

Fig. 3a represents the experiment conditions before the experiment was started. The thickness of the sedimentary cover layers from the bottom upward are: viscous layer 15mm, first sand layer 3mm, first plaster layer 3mm, second sand layer 10mm, rock powder 3mm, third sand layer 4mm, second plaster layer 3mm, and fourth sand layer 8mm. Therefore the total gravity force on the decollement surface is equal to:

$$W=142019.248 \text{ gr.cm.s}^{-2}$$

With 2cm shortening, the first thrust and back-thrust appeared and formed a box fold (Fig. 3b). As this thrust grew (Fig. 3c), its geometry shifted from a flat-ramp to a flat-ramp-flat. For this reason the related fold also changed from a thrust-tip-related fold to a thrust-step-related fold (at 3.5cm shortening). With further deformation, this trend was repeated for the second, third, fourth, and the fifth thrusts (Fig. 3d-3h), until at 18cm shortening, a back-thrust was formed in the fold related to the fifth thrust, and a triangular structure appeared (Fig. 3i). Fig. 3j shows that with creation of a small thrust at 22cm shortening, a small box fold was formed. This box fold and the thrust-related folds grew as the deformation reached 23.5cm shortening (Fig. 3k). When the deformation arrived at 28cm shortening, a thrust was formed at the end of the box (Fig. 3l). As we can see from Fig. 3m, this thrust along with its sixth back thrust, created a downthrown curved syncline region. The wavelength and amplitude of the anticlines related to each thrust are given in table 3

Table 3. Measurement of wavelength and amplitude anticlines

Shortening (cm)	Anticline 1		Anticline 2		Anticline 3	
	Wavelength (cm)	Amplitude (cm)	Wavelength (cm)	Amplitude (cm)	Wavelength (cm)	Amplitude (cm)
2	3	3.4				
3.5	8.4	6.5				
6.5	9	6.7				
9.5	7.4	7.2				
12	7.4	7.2				
13.5	11.6	7.7	11.2	3.6		
15.5	12	7.3	11	4.6		
18	11.7	7.4	11.6	5.6		
22	11.2	7	9.8	6.4	25.2	4.3
23.5	11	6.9	9	6.7	25.4	4
28	8	6.7	8.8	7.2	25.6	3.5
30	8.7	7.8	9	9	27.7	4.3

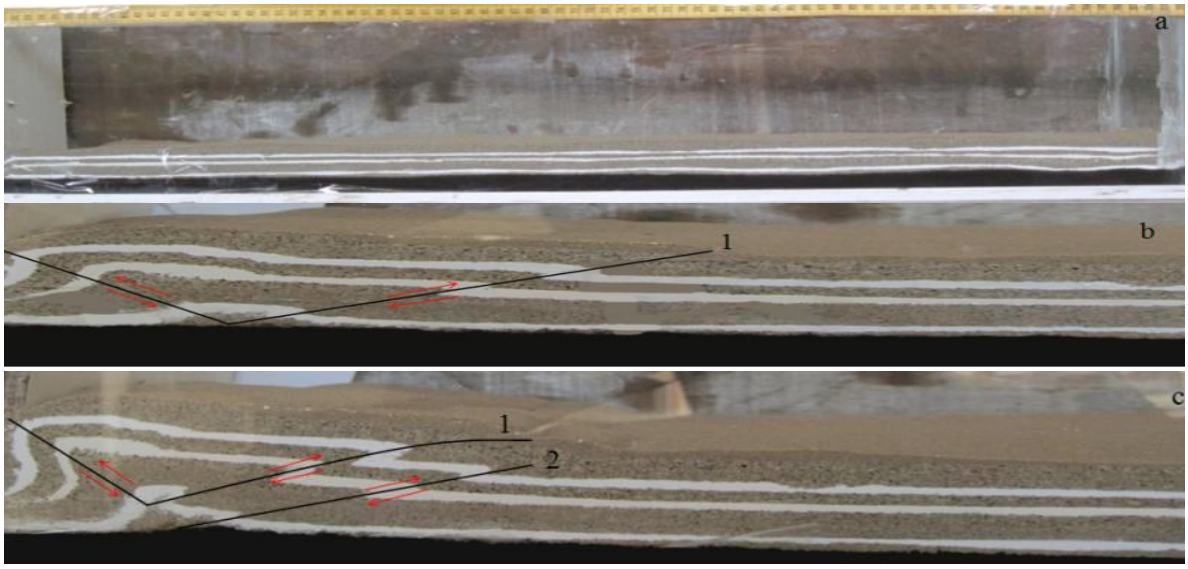

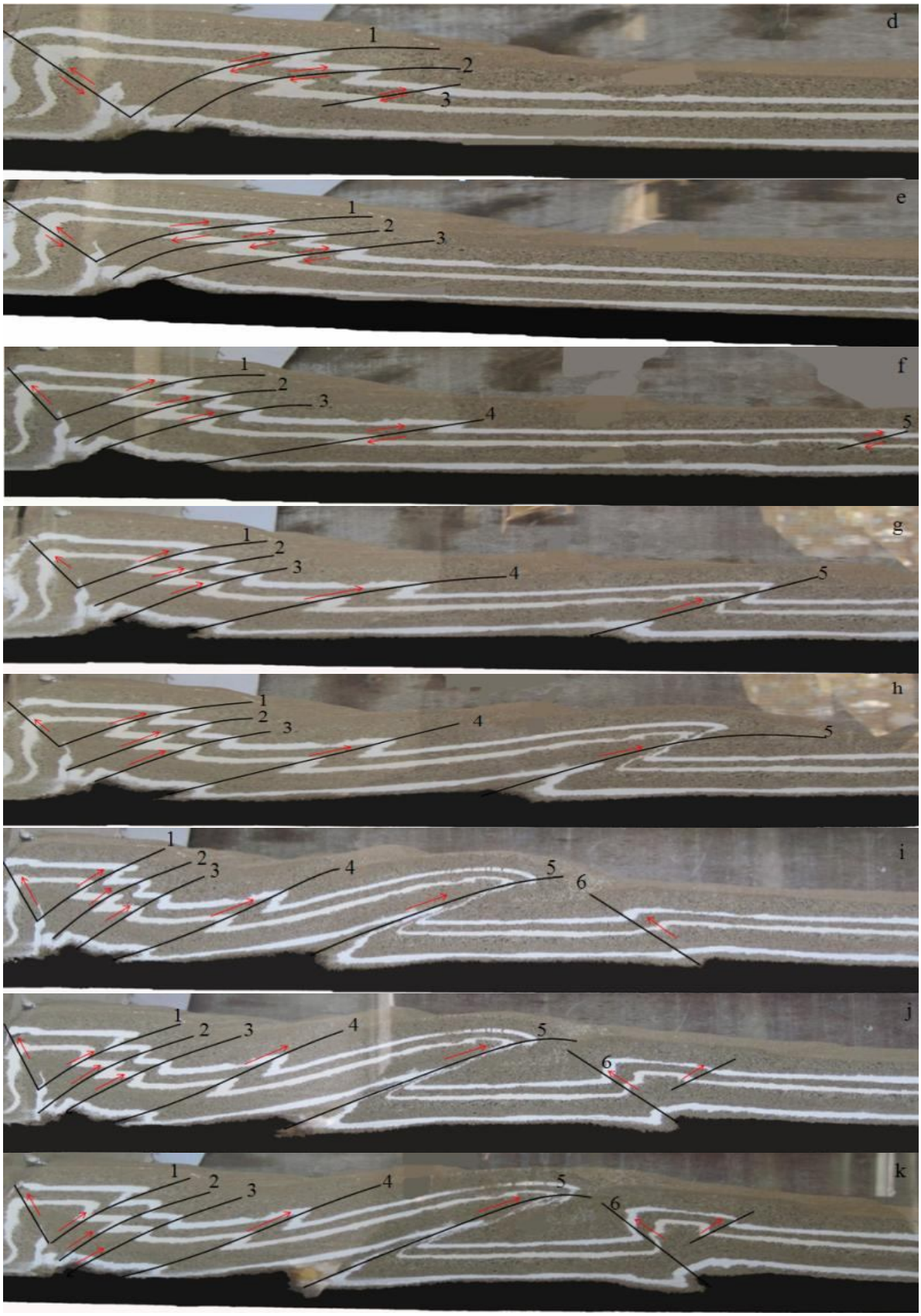
d
1
2
3
e
1
2
3
f
1
2
3
4
5
g
1
2
3
4
5
h
1
2
3
4
5
i
1
2
3
4
5
6
j
1
2
3
4
5
6
k
1
2
3
4
5
6

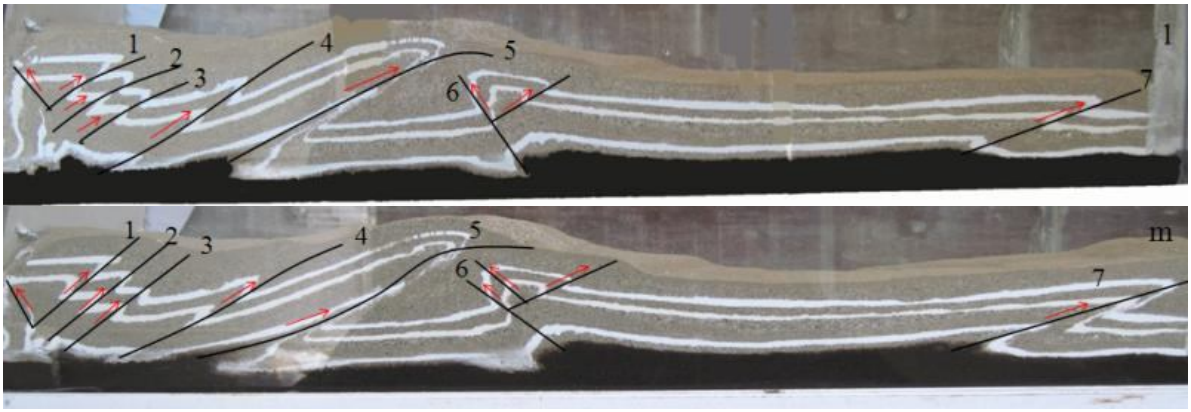

Fig. 4. Different stages of experiment F-3: a) The layered sedimentary sequence at the beginning of the experiment, b) formation of the first thrust and back thrust and creation of a box fold, c) the first thrust acquires a flat-ramp-flat geometry and the nucleation of the second thrust begins, d) nucleation of the third thrust, formation of the fold relevant to the second thrust step, and the second thrust gets a flat-ramp-flat geometry, e) formation of the fold relevant to the third thrust tip, f) nucleation of the fifth thrust, formation of the fold relevant to the fifth thrust, formation of the fold relevant to the fourth thrust tip, and creation of the piggy-back structures, g) formation of the fold relevant to the fifth thrust tip, h) the fifth thrust turns to flat-ramp-flat, and the anticline relevant to the step of this thrust is formed, i) nucleation of the sixth back thrust, j) formation of a small box fold on the fifth thrust step related anticline foreland, k) box fold development, l) nucleation of the seventh thrust, m) formation of the fold relevant to the tip the seventh thrust.

Experiment F-4

Fig. 5a represents the sequence of layers at the start of the experiment. The thickness of each layer in the box from the bottom upward are: viscous layer 10mm, first sand layer 5mm, first plaster layer 3mm, second sand layer 6mm, rock powder 4mm, third sand layer 8mm, second plaster layer 3mm, and fourth sand layer 5mm. The viscosity of the decollement surface is high. The total gravity force on the decollement surface is equal to:

$$W=142855.384 \text{ gr.cm.s}^{-2}$$

The first thrust and back-thrust appeared after 2cm shortening, together forming a box fold (Fig. 5b). Fig. 5c shows the next stage in the experiment, where growth of the thrust and back thrust further develop the box fold, and a second thrust was formed near the box fold. The geometry of this thrust at 7.5cm shortening was shifted from a flat-ramp to a flat-ramp-flat (Fig. 5d), and the fold related to it, was changed from a thrust-tip-related fold to a thrust-step-related one. Moreover the box fold became narrower. At this point of the experiment the viscous layer entered into the fold core. As the experiment continued, another thrust was formed parallel to the second thrust, and this trend was repeated for the third, fourth, fifth, sixth, and the seventh thrusts. Nevertheless the third and fourth thrusts were formed parallel and near to the two initial thrusts, while the fifth, sixth, and seventh thrusts were also formed parallel, to the initial thrusts, but farther away and in the foreland of the anticlines related to them (Fig. 5d-5k). In Fig. 5l, variations in uplift of the top sedimentary sequence layer at the final stage of the experiment is shown. The wavelength and amplitude of the anticlines created during this experiment are given in table 4.

Table4. Measurement of wavelength and amplitude anticlines

Shortening (cm)	Anticline 1		Anticline 2		Anticline 3	
	Wavelength(cm)	Amplitude(cm)	Wavelength(cm)	Amplitude(cm)	Wavelength (cm)	Amplitude (cm)
3	8.5	4.1				
6	14.2	6.2				
7.5	11.6	6.5				
10	11.2	6.7				
13	15.4	9				
15.5	23	8.8				
20	17.5	7.5				
22.5	19.2	8.5	8.7	4.5		
26.5	17.5	8.4	8.5	5	14.4	3.6
30	18	8.7	9	5.4	14	4

Accommodation of Doruneh anticline with the experimental model

Our study area is situated to the south of the Doruneh fault, in a sedimentary basin initially developed in the Oligocene-Miocene era. The basin is bounded by Foghan Mountain and the Gambi fault in south. Quaternary and Neogene deposits in the area are gentle folded, and from analysis of satellite imagery it is clear that the fold axes follows the trend of Doruneh fault (Fig. 1), which is divided into three segments trending NW-SE, E-W, and NE-SW from east to west. The large fault which controls the southern edge of sedimentary basin passes through the north of Foghan Mount in an east-west direction, and has brought Paleozoic sediments to the surface. In addition to the mentioned faults, there are several other fractures with the same trend as the main faults, and also numerous faults normal to these faults that were very likely created as a result of either main faults activities or fold curvature.

On the basis of field data the wavelength of folding decreases to the west whilst the fold amplitude increases. We interpret this variation in wavelength and amplitude to show that the Doruneh anticline initially formed in the eastern part and then propagated to the west (Fig. 6). At the final stage of test F-2, a few millimeters of the outer layer was taken off in order to expose the anticline core in the experiment (Fig. 7 and 8). The trend and axial surface of this anticline is identical to Kouche Mount's anticline.

CONCLUSION

Neogene and Quaternary deposits to the south of Kashmar have undergone folding. The analysis of satellite data indicates that the fold axes are parallel to the Doruneh strike-slip fault (Fig. 1). The Doruneh fault and the parallel folds are divided into three parts each with a different trend.

Three different trends of the Doruneh anticline are probably due to the action of north-south directed forces created as a result of the northward movement of the Lut block.

From analysis of field data and our experiment results, the folding appears to be propagating to the west. According to the field data, the middle part of the region, as illustrated in Fig. 6, is a downthrown in a synform situated between a thrust and a back thrust. The eastern part of the folds involves Kouche Mount whose axial surface corresponds to the anticline created from the fifth thrust in Fig. 4m. From the analysis of the field data and the experimental results, the western part of the anticline is related to thrusting. Putting these results together, we conclude that the Doruneh anticline is a thrust-related fold that has reached the Earth's surface in some places.

By analyzing the accomplished experiments, the effects of the controlling factors on deformation type caused by pressure acting parallel to the layering are as follows:

The effect of gravity force and the thickness variation of the sedimentary cover layers:

The effect of this factor is characterized by the comparison of the results from tests F-1 and F-4 with the results from tests F-2 and F-3. If the total thickness of the sedimentary cover is small, folding is dominant, and faulting will be dominant when the sedimentary cover thickness, and hence gravity force, is large.

Effect of the decollement surface viscosity and thickness

The effect of this factor is characterized by the comparison of the results from tests F-3 and F-4 with the results from tests F-1 and F-2. If the decollement surface viscosity is low, the sediments will generally be folded. However, when the decollement surface viscosity is high, faulting is the dominant deformation.

In all four tests, as the experiments progress, the fold wavelengths are decreased while the amplitudes are increased. The Doruneh anticlines show a westward decrease in wavelength and increase in amplitude and are thus likely to be propagating from east to west.

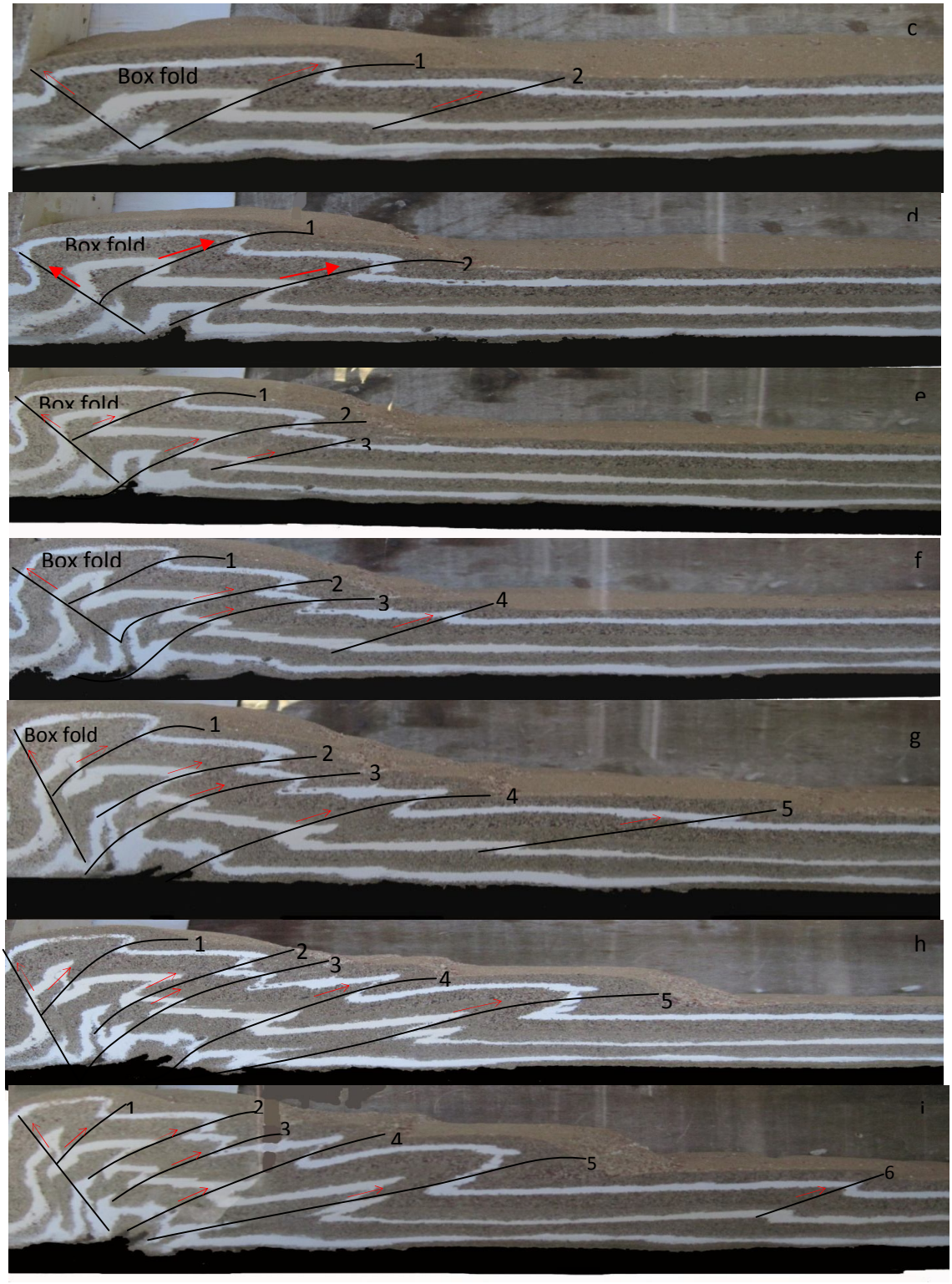
c
Box fold
1
2
d
Box fold
1
2
e
Box fold
1
2
3
f
Box fold
1
2
3
4
g
Box fold
1
2
3
4
5
h
1
2
3
4
5
i
1
2
3
4
5
6

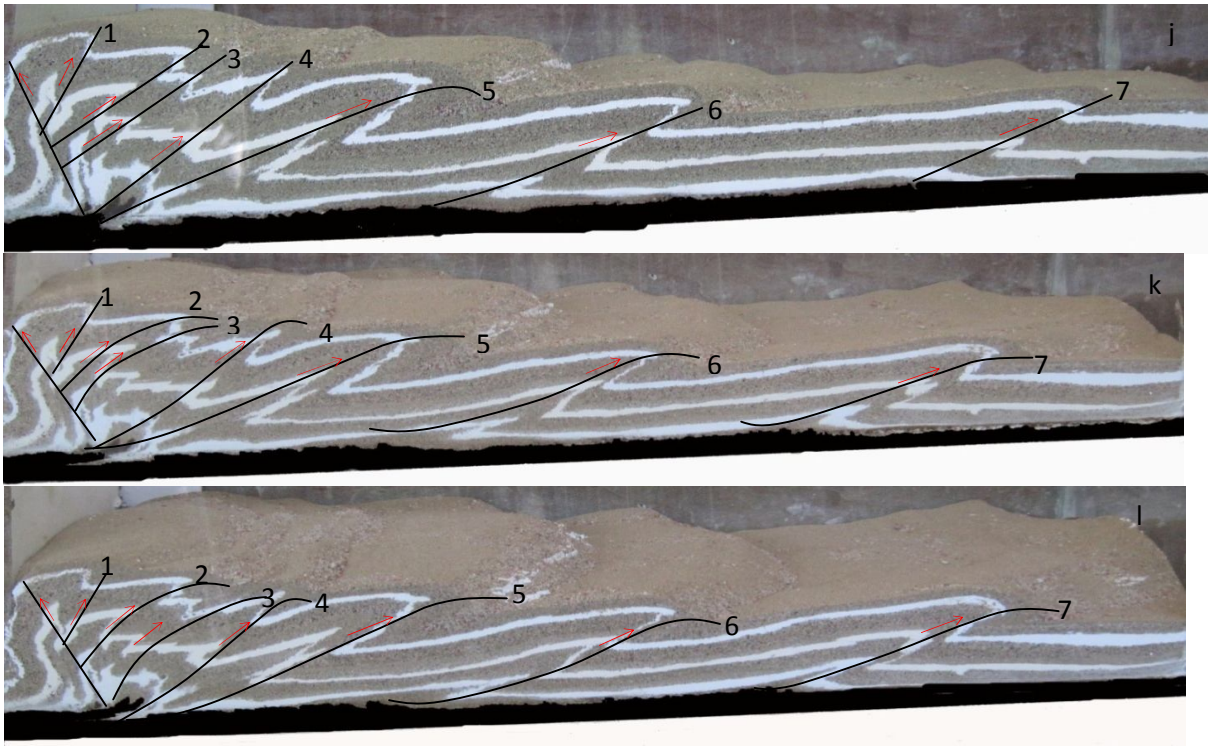

Fig. 5. Different stages of experiment F-4: a) The sedimentary layer sequence at the beginning of the experiment, b) formation of the first thrust and back thrust and creation of the box fold, c) the nucleation of the second thrust, d) the second thrust gets a flat-ramp-flat geometry, e) formation of the third thrust, f) nucleation of the fourth thrust and the third thrust gets a flat-ramp-flat geometry, g) formation of the fifth thrust and the fourth thrust gets a flat-ramp-flat, h) the fifth thrust turns to flat-ramp-flat, i) nucleation of the sixth thrust, j) nucleation of the seventh thrust and the sixth thrust gets a flat-ramp-flat geometry, k) the seventh thrust turns to flat-ramp-flat, l) variations in uplift of the top sedimentary sequence layer at the final stage of the experiment

Fig. 6: Comparison of the experimental model with the observed geometry of folding in the Doruneh anticline. The position of Fig. 7 is also specified in this Fig

.

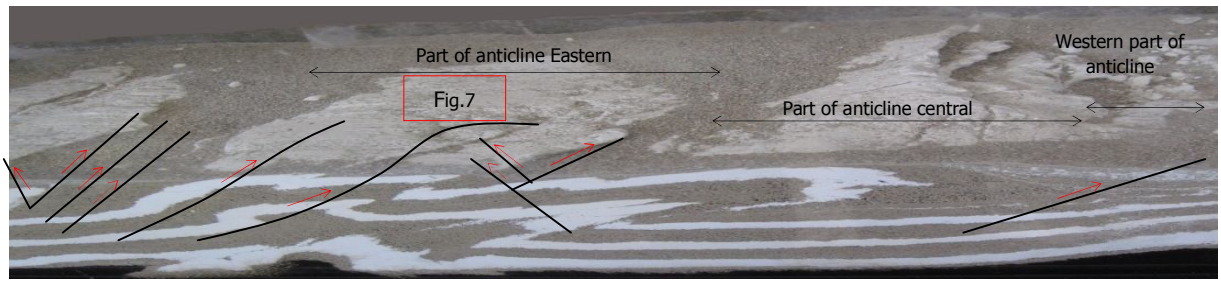

Fig. 7.An exposure of Koucheh Mount's anticline core.

Fig. 8. A close view of Koucheh Mount's anticline

ACKNOWLEDGMENTS

It is our pleasant duty to express my gratitude to those who have helped me with their advice and valuable comments on my work. We are kindly grateful to Dr. Richard Walker for editing this article. Our special thanks go to the department of geology of Sistan & Baluchestan University for supporting me during the whole period of my study.

REFERENCES

1. Stein. R., King. G.C.P. (1984). Seismic potential revealed by surface folding: the 1983 Coalinga, California. *Earthquake Science*. 224: 869–872.
2. Walker. R., Jackson. J., Baker. C. (2003). Thrust faulting in eastern Iran: source parameters and surface deformation of the 1978 Tabas and 1968 Ferdows earthquake sequences. Geophysical journal International. 157: 749-282.
3. Berberian. M. (1976). Contribution to the seism tectonics of Iran (Part II), Geological Survey of Iran, Report 39.
4. McClay. K.R. (1990). Deformation mechanics in analogue models of extensional fault systems. In Deformation Mechanisms, Rheology and Tectonics, Eds R. J. Knipe and E. H. Rutter, pp. 445453. Geological Society of London, Special Publication.
5. Suppe. J., Medwedeff. D.A. (1984). Geometry and kinematics of fault-propagation folding. *Eclogae geological* Helvetiae. 83: 909-954.
6. Mitra. S. (1990). Fault-propagation folds: geometry, kinematic evolution, and hydrocarbon traps, Bulletin of the American Association of Petroleum Geologists. 74: 921-945.
7. Salvini. F., Storti. F. (2001). The distribution of deformation in parallel fault- related folds with migrating axial surfaces: comparison between fault –propagation and fault-bend folding. *Journal of Structural Geology*. 23: 25–32.
8. Simpson. G.D.H. (2009). Mechanical modeling of folding versus faulting in brittle-ductile wedges. *Journal of Structural Geology* 31: 369-381.
9. Morley. C.K. (1994). Fold-generated imbricates: examples from the Caledonides of Southern Norway. *Journal of Structural Geology* 16: 619-631.
10. Hathaway. T.M., Gayer. R.A. (1995). 3-D geometry and displacement variation of thrust faults, terra abstracts (supplement to terra nova 7), 273.
11. Johnson. A.M. (1995). Orientation of faults determined by premonitory zones, shear tectonophisics. 247:161-238.
12. Storti. F., Salvini. F., Mcclay. K. (1997). Fault-related folding in sandbox analogue models of thrust wedges. *Journal of Structural Geology*. 19:583-602.

How to cite this article

Mohammad Mahdi Khatib, Tahereh Ghasemi and Mehrvash Nabiei. Geometrical Analysis of the Doruneh Anticline (South Kashmar, NE Iran) by Experimental Modeling. Bull. Env. Pharmacol. Life Sci., Vol 2 (10) September 2013: 67-78